

THE EVOLUTION OF THE ULTRALUMINOUS INFRARED GALAXY POPULATION FROM REDSHIFT 0 TO 1.5^{1,2}

L. L. COWIE,³ A. J. BARGER,^{4,5,3} E. B. FOMALONT,⁶ P. CAPAK³

Accepted by The Astrophysical Journal Letters

ABSTRACT

We use redshift observations of two deep 1.4 GHz fields to probe the evolution of the bright end of the radio galaxy luminosity function to $z = 1.5$. We show that the number of galaxies with radio power that would correspond locally to an ultraluminous infrared galaxy (ULIG) evolves rapidly over this redshift range. The optical spectra and X-ray luminosities are used to refine this result by separating the sources with clear active galactic nucleus (AGN) signatures from those that may be dominated by star formation. Both populations show extremely rapid evolution over this redshift range. We find that the number of sources with ULIG radio power and no clear AGN signatures evolves as $(1+z)^7$.

Subject headings: cosmology: observations — galaxies: distances and redshifts — galaxies: active — X-rays: galaxies — galaxies: formation — galaxies: evolution

1. INTRODUCTION

Star-forming ultraluminous infrared galaxies, or ULIGs ($L_{FIR} > 10^{12} L_{\odot}$ from Sanders & Mirabel 1996; here we mean galaxies without clear signatures of active galactic nucleus [AGN] activity in their spectra, even if there may be some AGN contribution to their luminosities), represent the most luminous tip of the star-forming galaxy population. Locally, ULIGs are very scarce (Kim & Sanders 1998), but if, as is widely believed, submillimeter galaxies are the high redshift analogs, then by $z = 1$ they are the dominant contributors to the star formation history (e.g., Lilly et al. 1999; Barger, Cowie, & Richards 2000; Gispert, Lagache, & Puget 2000; Chapman et al. 2003). It is extremely hard to trace the evolution of the ULIG population at low redshifts ($z < 1.5$) because of the difficulties of mapping large areas with current submillimeter detectors and of identifying the optical counterparts to low spatial resolution submillimeter or far-infrared (FIR) observations.

Ultradeep decimetric radio surveys can play a major, complementary role. The well-known tight correlation between FIR luminosity and radio power in local star-forming galaxies and radio-quiet AGNs (Condon 1992) means that we can identify ULIGs out to substantial redshifts based on their radio power. For a 1.4 GHz sensitivity limit of $40 \mu\text{Jy}$, an $L_{FIR} = 10^{12} L_{\odot}$ source will be detected to $z \sim 1.5$. Thus, sources with radio power that would correspond locally to a ULIG may be seen directly to large redshifts. Since the ultradeep 1.4 GHz samples cover large fields, do not suffer from extinction, and provide subarcsecond positional accuracy, it is easy to develop large samples with highly complete optical counterpart identifications.

By contrast, optically selected samples may omit dusty sources at these redshifts, while X-ray samples will select AGN dominated sources.

Current decimetric surveys do not probe the normal star-forming galaxy populations at $z = 1$. To the deepest 1.4 GHz sensitivity limits of $\sim 20 \mu\text{Jy}$ (5σ), a source with radio power corresponding to $L_{FIR} = 10^{10} L_{\odot}$ would only be seen to $z \sim 0.3$. Thus, attempts to provide maps of the entire star formation history over the $z = 0 - 1$ range based on decimetric observations (e.g., Cram 1998; Mobasher et al. 1999; Haarsma et al. 2000, hereafter H00) have to rely on model luminosity functions to extrapolate the measured data and obtain star formation rates. In these descriptions, much of the star formation lies in sources that are not directly measured by the observations (e.g., H00).

We use ultradeep 1.4 GHz observations of the Hubble Deep Field-North (HDF-N; Richards 2000) and SSA13 (Fomalont et al. 2004) fields to analyze the evolution of the radio luminosity function (LF) over the range $z = 0 - 1.5$. Our sample of 346 radio sources represents an increase of nearly a factor of five over H00 and enables us to provide a much more accurate determination of the $z = 1$ radio LF. We use optical spectral classifications and X-ray characteristics to separate AGN dominated sources from those that may be star formation dominated and to estimate the number density of ULIGs. An analysis of the submillimeter and far infrared properties of the sample will appear in Wang, Barger, and Cowie 2004 in preparation. We assume $\Omega_M = \frac{1}{3}$, $\Omega_{\Lambda} = \frac{2}{3}$, and $H_0 = 65 \text{ km s}^{-1} \text{ Mpc}^{-1}$.

2. SAMPLE

¹Based in part on data obtained at the W. M. Keck Observatory, which is operated as a scientific partnership among the the California Institute of Technology, the University of California, and NASA and was made possible by the generous financial support of the W. M. Keck Foundation.

²Based in part on data obtained at the VLA, which is a facility of the National Radio Astronomy Observatory (NRAO). The NRAO is a facility of the National Science Foundation operated under cooperative agreement by Associated Universities, Inc.

³Institute for Astronomy, University of Hawaii, 2680 Woodlawn Drive, Honolulu, HI 96822.

⁴Department of Astronomy, University of Wisconsin-Madison, 475 North Charter Street, Madison, WI 53706.

⁵Department of Physics and Astronomy, University of Hawaii, 2505 Correa Road, Honolulu, HI 96822.

⁶National Radio Astronomy Observatory, Charlottesville, VA 22903.

Richards (2000) presented a catalog of 1.4 GHz sources detected in a Very Large Array (VLA) map centered on the HDF-N that covers a $40'$ diameter region with an effective resolution of $1.8''$. The 5σ completeness limit for compact sources in the central region of the map is $40 \mu\text{Jy}$. Fomalont et al. (2004) presented a similar catalog within a $17'$ radius of the 1.4 GHz VLA map (5σ completeness of $25 \mu\text{Jy}$) of the SSA13 field (R.A. = $13^{\text{h}}23^{\text{m}}$, decl. = $42^{\circ}38''$). In both cases, the completeness limits for more extended sources are several times higher. The absolute radio positions are known to $0.1'' - 0.2''$ rms. Optical imaging data for the two fields can be found in Capak et al. (2003) and Barger et al. (2001), respectively. Alexander et al. (2003) presented 2 Ms *Chandra* Deep Field-North (CDF-N) X-ray images that cover about 460 arcmin^2 around the HDF-N. Near the aim point, the data reach limiting fluxes of $\approx 1.5 \times 10^{-17}$ ($0.5 - 2 \text{ keV}$) and $\approx 10^{-16} \text{ ergs cm}^{-2} \text{ s}^{-1}$ ($2 - 8 \text{ keV}$). Mushotzky et al. (2000) and Barger et al. (2001) presented 100 ks *Chandra* exposures of the SSA13 field with limiting fluxes 20 times higher than the CDF-N.

For the HDF-N region, we use a $9.3'$ radius area around the approximate *Chandra* image center R.A. = $12^{\text{h}} 36^{\text{m}} 51.20^{\text{s}}$ and decl. = $62^{\circ}13' 43.0''$ (J2000.0). The $9.3'$ radius is the largest circle that can be drawn within the *Chandra* area. 195 of the 372 radio sources lie within this circle. For the SSA13 field, we use a rectangular area of 175 arcmin^2 that contains 221 sources. We have so far spectroscopically observed 154 of these sources, chosen without regard to their radio or optical properties; thus, the effective area is 120 arcmin^2 . Together these two restricted samples constitute our radio sample with 346 sources. All lie well within the half power radius of the radio observations, so the two fields should have relatively uniform flux selections.

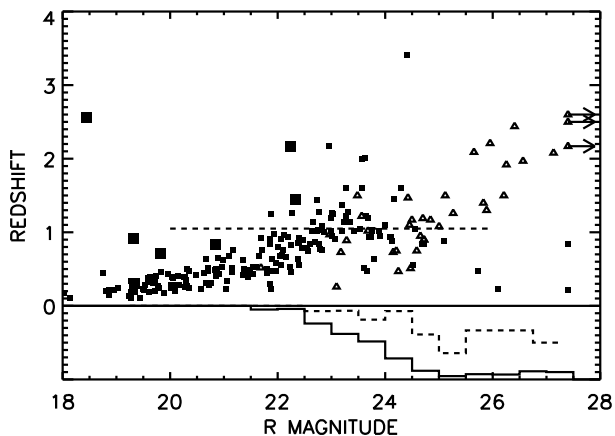


FIG. 1.— Redshift versus R magnitude for our radio sample, excluding the two spectroscopically identified stars (*solid squares*—spectroscopic redshifts; *open triangles*—photometric redshifts; *large solid squares*—broad-line AGNs). Dashed horizontal line shows the redshift ($z = 1.05$) for which a source with the median radio flux of $80 \mu\text{Jy}$ would have a radio power that would correspond locally to a ULIG. Solid histogram shows the spectroscopic completeness: at $R < 23$, 96% (152 of the 162 sources) are identified; at $R = 23.5 - 24$, just over 50%; at fainter magnitudes, only a handful with strong emission lines. Dashed histogram shows the completeness of the combined photometric and spectroscopic redshifts in the HDF-N: 92% of the $R < 25$ sources have either a spectroscopic or a photometric redshift.

We observed our radio sample with the Deep Extragalactic Imaging Multi-Object Spectrograph (DEIMOS; Faber et al. 2003) on the Keck II 10 m telescope and the Low-Resolution Imaging Spectrograph (LRIS; Oke et al. 1995) on Keck I. We spectroscopically identified 192 of the 346 sources (55%), two of which are stars. Figure 1 shows spectroscopic redshift versus R magnitude (*solid symbols*) for our radio sample, as well as the completeness of our spectroscopic identifications versus R magnitude (*solid histogram*). A source with the median radio flux of $80 \mu\text{Jy}$ has a radio power corresponding to a local ULIG at $z = 1.05$ (*dashed horizontal line*); this corresponds to R magnitudes in the range 22.5 to 25 (see Fig. 1). Spectroscopic identifications can be obtained for the majority of sources to $R = 24$ and for some in the $R = 24$ to $R = 25$ range (see *solid histogram*).

We can also estimate redshifts from photometric colors. For the HDF-N, we use the photometric redshifts of Capak et al. (2004), which are based on ultradeep imaging in seven colors from U to HK' (Capak et al. 2003) and were computed using the Bayesian code of Benítez (2000). This code assigns odds that the redshift lies close to the estimated value; we only use cases with odds above 90%. The imaging data saturate at bright magnitudes, so we restrict to sources with $R > 20$, leaving 161 photometric redshifts. The photometric redshifts (*open triangles*) for sources that do not also have spectroscopic redshifts are shown in Figure 1, as is the completeness of our HDF-N combined photometric and spectroscopic redshift sample versus R magnitude (*dashed histogram*). Eighty-three sources with $R > 20$ have both spectroscopic and photometric redshifts, and 92% of these agree to within a multiplicative factor of 1.25. This agreement is independent of spectral type, except for the very small number of broad-line AGNs, where the failure rate is higher. The success rate of the photometric redshifts is consistent with that expected from the assigned odds. Since we do not have photometric redshifts for the SSA13 sources, and since photometric redshifts do not contain spectral type information, we only use the photometric redshifts to test the effects of completeness on the total LF.

For the spectroscopically identified sources, we classified the optical spectra into four spectral types, roughly following the procedure used by Sadler et al. (2002, hereafter S02) to analyze low redshift 1.4 GHz samples. We classified sources without strong emission lines ($\text{EW}([\text{OII}]) < 3 \text{ \AA}$ or $\text{EW}(\text{H}\alpha + \text{NII}) < 10 \text{ \AA}$) as absorbers; sources with strong Balmer lines and no broad or high-ionization lines as star formers; sources with $[\text{NeV}]$ or CIV lines or strong $[\text{OIII}]$ ($\text{EW}([\text{OIII}] 5007 \text{ \AA}) > 3 \text{ EW}(\text{H}\beta)$) as Seyferts; and, finally, sources with $\text{FWHM} > 1000 \text{ km s}^{-1}$ as broad-line AGNs. The breakdown by spectral type in each field, and also by radio flux, is given in Table 1. S02 argued that the absorbers must be AGN dominated since star formation cannot produce the synchrotron emission in these galaxies. They combined all but the star formers into a single AGN class.

The deep CDF-N X-ray data provide a check and a refinement of the classifications. We computed the $2 - 8 \text{ keV}$ rest-frame luminosity, L_x , for each source with a spectroscopic redshift. In Figure 2 we plot L_x versus radio power for the AGNs (classes 3 and 4; *triangles*), the star form-

ers (*diamonds*), and the absorbers (*squares*). The sources classed as AGNs are generally X-ray luminous. Of the 40 AGNs, 29 are detected in the 2–8 keV band, 26 of which have $L_x > 10^{42}$ ergs s $^{-1}$. Such luminosities would securely identify them as AGNs (Zezas, Georgantopoulos, & Ward 1998; Moran, Lehnert, & Helfand 1999). The remaining upper bounds are consistent with all of the sources having $L_x > 10^{41}$ ergs s $^{-1}$.

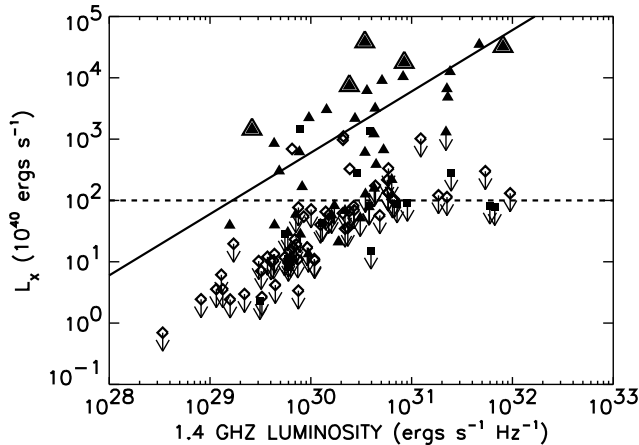


FIG. 2.— 2–8 keV luminosity versus 1.4 GHz power for the HDF-N radio sample. Triangles show sources with AGN optical spectra (*large symbols*—broad-line AGNs; *small symbols*—Seyferts); diamonds show star formers; squares show absorbers. Arrows denote upper limits for sources not detected in the 2 Ms CDF-N. Solid diagonal line is an approximate linear fit to the AGN population and is just shown for guidance. Dashed horizontal line shows the luminosity that would securely identify a source as an AGN.

By contrast, nearly all of the star formers have low X-ray luminosities. Only six of the 55 sources are detected in the 2–8 keV band, and only four have $L_x > 10^{42}$ ergs s $^{-1}$. The absorbers are the most unusual class. If they are AGN dominated, then they are very underluminous in their rest-frame 2–8 keV luminosities relative to their radio power. This suggests that they could be Compton-thick or near Compton-thick sources. It may therefore be useful to maintain the distinction between the AGNs with clear optical signatures and the absorbers. However, to be consistent with S02, we combine the two classes. The absorbers class has about half as many sources as the spectroscopic AGN class and a similar distribution of radio power. Thus, the AGN radio LF may be roughly corrected to a spectroscopic AGN LF by multiplying by 0.66. Some sources that have star-forming optical signatures may also correspond to this type of source: X-ray quiet, radio detected AGN with no spectroscopic AGN signatures. There may be ongoing star formation in the galaxy, but the AGN dominates the radio power. Thus, the optically classified star formers may only be an upper limit to the population where star formation dominates the radio power.

For our final classification, we classed all absorbers, star formers known to have measured (not limits) $L_x > 10^{42}$ ergs s $^{-1}$, and sources with AGN optical spectra as AGNs. We classed the remaining sources as star formers. This enables straightforward comparisons with the local results of Condon (1989), Condon, Cotton, & Broderick (2002), Machalski & Godlowski (2001, hereafter MG01), and S02.

3. DISCUSSION

We constructed the LFs for the 1.4 GHz power over the range $z = 0.5 - 1.5$ using the $1/V_a$ method (e.g., Felten 1977). This is shown for the total spectroscopic sample (AGNs and star formers; *triangles*) in Figure 3a, where it is compared with the local measurements of Condon (1989; *solid line*). To investigate the effects of incompleteness, we computed the maximum total LF (*squares*) for just the HDF-N using the much more complete combined photometric and spectroscopic samples and placing all sources without a photometric or a spectroscopic redshift into the $z = 0.5 - 1.5$ bin. Many of these probably lie at higher redshifts, so this is an upper bound. Finally, we assumed that the HDF-N sample was only 50% complete in the 40–80 μ Jy range, which approximates the completeness corrections computed by Richards (2000). The maximum correction for incompleteness is a factor of 2.6 at the lower radio powers but is relatively small at the higher radio powers.

In order to parameterize the evolution, we assumed that the local portion of the LF allocated to star formers in Condon (1989) undergoes pure luminosity evolution and that allocated to AGNs undergoes pure number density evolution. We used these assumptions to calculate the expected LF in the $z = 0.5 - 1.5$ interval. (The use of the S02 or the MG01 measurements, which were constructed using more similar methodologies to ours for classifying the galaxies, does not change the diagrams significantly.) This simple model provides a reasonable fit to our measured LF, with the AGN number density evolving as $(1+z)^3$, and the star-forming luminosities evolving as either $(1+z)^3$ (*dotted line*), if we match the observed LF, or as $(1+z)^{3.8}$ (*dashed line*), if we match the maximum total LF. This systematic uncertainty is much larger than the statistical errors and primarily affects the evolution of the star-forming LF because the uncertainties are larger at the lower luminosities where this term dominates. Our results for the evolution of the star-forming LF are consistent with those determined from local samples by MG01 and Condon et al. (2002), who found a similar evolution of $(1+z)^{3\pm 1}$. Our results are also broadly consistent with those of H00, who found a best pure luminosity evolution model with $(1+z)^{2.9}$.

In Figures 3b and 3c we show the measured LFs in two narrower intervals ($z = 0.6 - 0.9$ and $z = 0.9 - 1.4$, respectively, chosen to match H00) and by spectroscopic class (*diamonds*—star formers; *squares*—AGNs). For the star formers, we also show the results of H00 (*triangles*), which, within the uncertainties, agree with the present measurements. Our results are again broadly consistent with the evolution described above (see Fig. 3b caption for description), although the AGN LF is slightly high in the $z = 0.6 - 0.9$ interval. This suggests that the power law evolution model may be too simple and that the evolution of the AGN LF is faster at low redshifts and slower at high redshifts. The star formers begin to show a more extended high luminosity tail in the $z = 0.9 - 1.4$ interval.

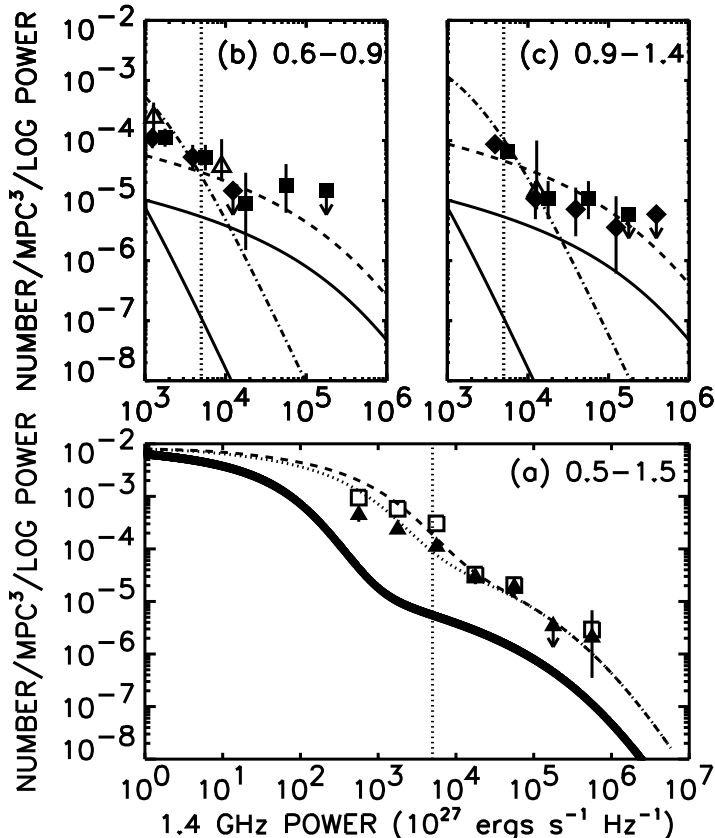


FIG. 3.— (a) Radio LF at $z = 0.5 - 1.5$ for all the spectroscopically identified radio sources (*triangles*), compared with the local determination from Condon (1989; *solid line*). Log denotes the base 10 logarithm. The 1σ uncertainties are Poissonian. Squares denote the maximum total LF. Vertical dotted line shows the equivalent radio power of an $L_{FIR} = 10^{12} L_{\odot}$ source. Dotted curve shows the expected LF if the local star-forming LF undergoes pure luminosity evolution $((1+z)^3)$ and the local AGN LF undergoes pure number density evolution $((1+z)^3)$. Uncertainties are primarily systematic, and luminosities evolving as $(1+z)^{3.8}$ provide a better fit (*dashed line*) to the maximum total LF. (b) Radio LF at $z = 0.6 - 0.9$ for the star formers (*diamonds*) and the AGNs (*squares*), to be compared with the local star former (*steep solid curve*) and AGN (*shallow solid curve*) determinations from Condon (1989). Triangles show the measurements of H00 (with a small correction to make the geometries consistent) for the star formers. Dot-dashed curve shows the expected LF if the local star-forming LF undergoes pure luminosity evolution $((1+z)^{3.8})$. Dashed curve shows the expected LF if the local AGN LF undergoes pure number density evolution $((1+z)^3)$. (c) As for (b), but for the $z = 0.9 - 1.4$ redshift interval.

The rapid evolution of the radio LF implies that the number density of very luminous sources rises rapidly in the $z = 0 - 1$ interval for both the star former and AGN classes though it may be beginning to slow at redshifts $z > 1$. In Figure 4 we show the number density of star formers with ULIG radio power (*solid squares*) in three redshift intervals. The value from the local star-forming radio LF is given by the open square. The evolution is reasonably well described by a $(1+z)^7$ evolution (*dashed line*). This evolution is similar to that inferred by Barger et al. (2000) from a comparison of the local number density of ULIGs and near-ULIGs to the $z = 1 - 3$ number density of > 6 mJy radio/submillimeter sources (*solid circle*). If most of the submillimeter sources are dominated by star

formation (Barger et al. 2000; Chapman et al. 2003), the match to the radio evolution is reasonable, if the radio galaxies classified as star formers are indeed dominated by star formation and the FIR-radio correlation holds to these redshifts as suggested by recent results (Garrett 2002).

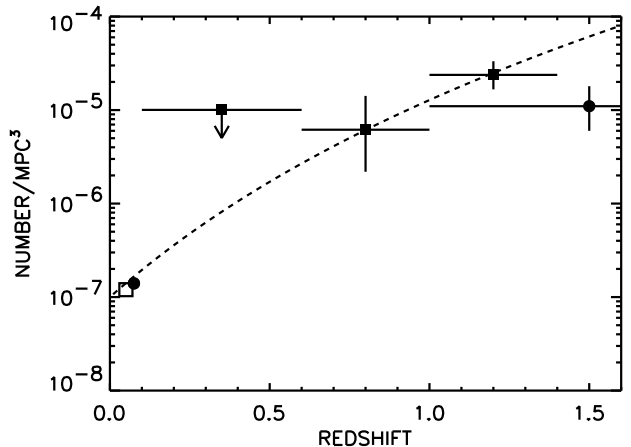


FIG. 4.— Number density of star formers with ULIG radio power in the redshift intervals $z = 0.1 - 0.6$, $z = 0.6 - 1.0$, and $z = 1.0 - 1.4$ (*solid squares*). Open square denotes the value from the local star-forming radio LF. Solid circles denote the local number density of ULIGs and near-ULIGs and the $z = 1 - 3$ number density of > 6 mJy radio/submillimeter sources (from Barger et al. 2000). Dashed line shows a $(1+z)^7$ evolution.

4. SUMMARY

We have given a precise determination of the high power end of the radio LF at high redshifts ($z \sim 1$). The LF was shown to evolve rapidly with redshift, both for galaxies with AGN spectra and for those with only star-forming signatures. This result is consistent with model expectations based on the local LF and the radio number counts (e.g., Condon 1989). The number of sources with radio luminosities that would correspond to ULIGs (based on local normalizations) matches the observed evolution from the local ULIG population to the radio/submillimeter sources at $z > 1$.

We thank the referee for helpful comments that improved the manuscript. L. L. C. gratefully acknowledges support from NASA grants GO2-3187B and HST-GO-09425.03-A and NSF grant AST-0084816, and A. J. B. from NASA grant HST-GO-09425.30-A, NSF grant AST-0084847, NSF CAREER award AST-0239425, the UW Research Committee, the Alfred P. Sloan Foundation, and the David and Lucile Packard Foundation.

REFERENCES

- Alexander, D. M., et al. 2003, *AJ*, 126, 539
 Barger, A. J., Cowie, L. L., Mushotzky, R. F., & Richards, E. A. 2001, *AJ*, 121, 662
 Barger, A. J., Cowie, L. L., & Richards, E. A. 2000, *AJ*, 119, 2092
 Benítez, N. 2000, 536, 571
 Capak, P., et al. 2003, *AJ*, 127, 180
 Capak, P., et al. 2004, in preparation
 Chapman, S. C., Blain, A. W., Ivison, R. J., & Smail, I. 2003, *Nature*, 422, 695
 Condon, J. J. 1989, *ApJ*, 338, 13
 Condon, J. J. 1992, *ARA&A*, 30, 575
 Condon, J. J., Cotton, W. D., & Broderick, J. J. 2002, *AJ*, 124, 675
 Cram, L. E. 1998, *ApJ*, 506, L85
 Faber, S. M., et al. 2003, *Proc. SPIE*, 4841, 1657
 Felten, J. E. 1977, *AJ*, 82, 861
 Fomalont, E. B., Kellermann, K. I., Cowie, L. L., Barger, A. J., Capak, P., Partridge, R. B., & Windhorst, R. A. 2004, *ApJ*, in preparation
 Garrett, M.A. 2002, *A&A*, 384, L19
 Gispert, R., Lagache, G., & Puget, J. L. 2000, *A&A*, 360, 1
 Haarsma, D. B., Partridge, R. B., Windhorst, R. A., & Richards, E. A. 2000, *ApJ*, 544, 641 (H00)
 Kim, D.-C., & Sanders, D. B. 1998, *ApJS*, 119, 41
 Lilly, S. J., et al. 1999, *ApJ*, 518, 641
 Machalski, J., & Godlowski, W. 2001, *A&A*, 370, 923 (MG01)
 Mobasher, B., Cram, L., Georgakakis, A., & Hopkins, A. 1999, *MNRAS*, 308, 45
 Moran, E. C., Lehnert, M. D., & Helfand, D. J. 1999, *ApJ*, 526
 Mushotzky, R. F., Cowie, L. L., Barger, A. J., & Arnaud, K. A. 2000, *Nature*, 404, 459
 Oke, J. B., et al. 1995, *PASP*, 107, 375
 Richards, E. A. 2000, *ApJ*, 533, 611
 Sadler, E. M., et al. 2002, *MNRAS*, 329, 227 (S02)
 Sanders, D. B., & Mirabel, I. F. 1996, *ARA&A*, 34, 749
 Zezas, A., Georgantopoulos, I., & Ward, M. J. 1998, *MNRAS*, 30

TABLE 1
 BREAKDOWN OF SPECTRAL TYPE BY FIELD AND RADIO FLUX (μ JY)

CATEGORY	HDF	SSA13	ALL	25-50	50-100	100-200	> 200
total	195	151	346	37	186	77	46
identified	115	82	197	20	98	51	28
stars	0	2	2	0	2	0	0
absorbers	15	14	29	1	16	4	8
star formers	57	49	106	10	51	33	12
Seyferts	36	13	49	8	23	12	6
broad-line	5	3	8	0	5	1	2